

## Control of Magnetocrystalline Anisotropy by Epitaxial Strain in Double Perovskite $\text{Sr}_2\text{FeMoO}_6$ Films

Chunhui Du, Rohan Adur, Hailong Wang, Adam J. Hauser, Fengyuan Yang,<sup>\*</sup> and P. Chris Hammel<sup>†</sup>

*Department of Physics, The Ohio State University, 191 West Woodruff Avenue Columbus, Ohio 43210, USA*

(Received 7 January 2013; published 2 April 2013)

We demonstrate tuning of magnetocrystalline anisotropy in high-quality  $\text{Sr}_2\text{FeMoO}_6$  epitaxial films over a range of several thousand Gauss using strain induced by epitaxial growth on substrates of varying lattice constants. Spectroscopic measurements reveal a striking, linear dependence of the out-of-plane anisotropy on the strain-induced tetragonal distortion of the  $\text{Sr}_2\text{FeMoO}_6$  lattice. This anisotropy can be tuned from +2000 to −3300 Oe, a range sufficient to rotate the easy axis from in plane to out of plane. Combined with its half-metallicity and high Curie temperature, this result implies a broad range of scientific and technological applications for this novel spintronic material.

DOI: [10.1103/PhysRevLett.110.147204](https://doi.org/10.1103/PhysRevLett.110.147204)

PACS numbers: 75.30.Gw, 75.70.Tj, 76.50.+g

Magnetization orientation is widely used for information processing and storage applications [1]. There is widespread interest in discovering methods that could grant efficient, local control of magnetization. Ferro- or ferri-magnets (FM) with a strong magnetocrystalline anisotropy, in which spin-orbit interactions couple magnetization to a crystalline structure, offer a promising route to achieving this capability. High-quality epitaxial FM films are desirable for technological applications using strain-tunable magnetocrystalline anisotropy to control magnetization orientation. Half-metallic double perovskite  $\text{Sr}_2\text{FeMoO}_6$  (SFMO) is an attractive material [2–10] for the study and application of magnetocrystalline anisotropy due to its high spin polarization, high Curie temperature ( $T_C$ ) (well above room temperature), and relatively strong spin-orbit coupling provided by the  $4d$  transition metal Mo.

We have succeeded in growing high-quality  $\text{Sr}_2\text{FeMoO}_6$  epitaxial films [10] that, in addition to enabling detailed studies, provide a robust platform for technological applications. The fabrication of  $\text{Sr}_2\text{FeMoO}_6$  epitaxial films [6–10] has been extensively studied. However, their chemical complexity and strict reduction or oxidation requirements make it very difficult to deposit  $\text{Sr}_2\text{FeMoO}_6$  films of sufficient quality to reveal intrinsic properties [11–13]. Moreover, almost all reported  $\text{Sr}_2\text{FeMoO}_6$  film fabrication has employed a single substrate,  $\text{SrTiO}_3$  (STO), for which the lattice mismatch  $\eta = (a_s - a_f)/a_f$  with  $\text{Sr}_2\text{FeMoO}_6$  is −1.1%, where  $a_s$  and  $a_f$  are the in-plane lattice constants of the substrate and unstrained films, respectively. Given the relatively strong spin-orbit coupling in  $\text{Sr}_2\text{FeMoO}_6$ , one may expect magnetocrystalline anisotropy to be sensitive to structural distortion that can be induced and controlled by epitaxial strain. In particular, this can enable the large strain-induced out-of-plane magnetocrystalline anisotropy needed to produce perpendicularly magnetized FM films that can serve as perpendicular polarizers for a spin-transfer-torque device with low critical current [14] for nonvolatile memory [15] and spin-torque oscillator

devices [16]. Shape anisotropy dictates in-plane magnetization for most FM films, while only a handful of films and heterostructures exhibit out-of-plane anisotropy. Continuous strain control of magnetocrystalline anisotropy promises to expand the family of such films available for strain-tuned magnetization as well as perpendicular polarizers. Magnetocrystalline anisotropy has been investigated in thin films of metals, dilute magnetic semiconductors, and  $\text{La}_{0.7}\text{Sr}_{0.3}\text{MnO}_3$  [17–21]. Tunable magnetic anisotropy was observed below 100 K in  $\text{GaMnAs}$  by epitaxial strain [19] and in  $\text{GaMnAsP}$  by varying the phosphorous content [20]. However, the correlation between magnetic anisotropy and strain-induced lattice distortion has not been systematically studied. Here we report growth of  $\text{Sr}_2\text{FeMoO}_6$  epitaxial films on a selected set of single-crystal substrates and buffer layers to create a range of strain-induced tetragonal distortion in  $\text{Sr}_2\text{FeMoO}_6$  films and measurements of their out-of-plane magnetocrystalline anisotropy by ferromagnetic resonance (FMR).

Epitaxial  $\text{Sr}_2\text{FeMoO}_6$  films with thicknesses  $t$  varying from 50 to 200 nm were grown using a new sputtering technique [10,22,23]; this range of thicknesses spans from fully strained (50 nm) to nearly relaxed (200 nm) films. For  $\text{Sr}_2\text{FeMoO}_6$  films below 50 nm, the average film quality decreases because it takes several nm to fully establish the Fe/Mo ordering during early stages of film growth, resulting in an Fe/Mo disordered layer several nm thick near the interface. Four different (001)-oriented substrates or buffer layers have been used to enable tuning of the lattice mismatch with  $\text{Sr}_2\text{FeMoO}_6$  (bulk  $a = 3.947$  Å): (1)  $\text{SrTiO}_3$ , (2) a fully strained  $\text{Sr}_2\text{CrNbO}_6$  (SCNO) buffer layer on  $\text{SrTiO}_3$ , (3) a  $\text{Sr}_2\text{GaTaO}_6$  (SGTO) buffer layer on  $\text{SrTiO}_3$ , and (4) a fully relaxed  $\text{Sr}_2\text{CrNbO}_6$  buffer layer on  $(\text{LaAlO}_3)_{0.3}(\text{Sr}_2\text{AlTaO}_6)_{0.7}$  (LSAT). The lattice constants of the four substrates or buffer layers were measured by high resolution x-ray diffraction (XRD); the lattice mismatch and the sign of the strain with respect to  $\text{Sr}_2\text{FeMoO}_6$  are shown in Table I. All buffer layers are

TABLE I. Lattice parameters, lattice mismatch and sign of strain due to buffer layers and substrates used to grow epitaxial  $\text{Sr}_2\text{FeMoO}_6$  (bulk  $a = c = 3.947 \text{ \AA}$ ) films.

Buffer layer/Substrate	$a(=b)$ ( $\text{\AA}$ )	$c$ ( $\text{\AA}$ )	Lattice mismatch	Sign of strain
$\text{SrTiO}_3$	3.905	3.905	-1.1%	Compressive
$\text{Sr}_2\text{GaTaO}_6/\text{SrTiO}_3$	3.970	3.970	0.58%	Tensile
$\text{Sr}_2\text{CrNbO}_6/\text{LSAT}$	3.950	3.944	0.076%	Tensile
$\text{Sr}_2\text{CrNbO}_6/\text{SrTiO}_3$	3.905	3.988	-1.1%	Compressive

around 100 nm thick. The magnetizations of the films were measured using a superconducting quantum interference device (SQUID) magnetometer and a vibrating sample magnetometer (VSM).

XRD clearly demonstrates the importance of a substrate or buffer layer on the crystalline quality and strain relaxation of the  $\text{Sr}_2\text{FeMoO}_6$  films. Figure 1 shows representative  $\theta$ - $2\theta$  scans of the  $\text{Sr}_2\text{FeMoO}_6$  films with  $t = 100$  and 200 nm grown on  $\text{SrTiO}_3$ ,  $\text{Sr}_2\text{CrNbO}_6/\text{LSAT}$ , and  $\text{Sr}_2\text{GaTaO}_6/\text{SrTiO}_3$ . For  $\text{Sr}_2\text{FeMoO}_6$  films grown on  $\text{SrTiO}_3$  [Fig. 1(a)], the relatively large lattice mismatch ( $\eta = -1.1\%$ , compressive) elongates the out-of-plane lattice constant  $c$ , resulting in a tetragonal distortion. The in-plane lattice constants  $a(=b)$  were measured using off-axis XRD scans on the  $\text{Sr}_2\text{FeMoO}_6$  (022) peaks. The tetragonal distortion (tetragonality  $\sigma = (c - a)/a$ ) decreases from 1.7% for the 100-nm-thick film

( $a = 3.915 \text{ \AA}$ ,  $c = 3.981 \text{ \AA}$ ) to 0.41% for the 200-nm film ( $a = 3.941 \text{ \AA}$ ,  $c = 3.957 \text{ \AA}$ ).

The  $\text{Sr}_2\text{CrNbO}_6$  buffer layers grown on LSAT ( $a = 3.868 \text{ \AA}$ ) are fully relaxed for all thicknesses [Fig. 1(b)] due to the larger lattice mismatch between bulk  $\text{Sr}_2\text{CrNbO}_6$  ( $a = 3.944 \text{ \AA}$ ) and LSAT. Because the in-plane lattice constants of  $\text{Sr}_2\text{CrNbO}_6$  and  $\text{Sr}_2\text{FeMoO}_6$  are nearly identical, the  $\text{Sr}_2\text{FeMoO}_6$  films on  $\text{Sr}_2\text{CrNbO}_6/\text{LSAT}$  are essentially strain free. These samples serve as the ‘‘origin’’ in the strain tuning of the magnetoelastic coupling. The  $\text{Sr}_2\text{FeMoO}_6$  films grown on  $\text{Sr}_2\text{GaTaO}_6$  buffer layers ( $a = c = 3.970 \text{ \AA}$ ,  $\eta = +0.58\%$ ) on  $\text{SrTiO}_3$  [Fig. 1(c)] show a small tetragonal distortion with an expanded  $a = 3.963 \text{ \AA}$  and a compressed  $c = 3.935 \text{ \AA}$  for the 200-nm-thick film. The satellite peaks in Figs. 1(b) and 1(c) are XRD Laue oscillations, which indicate highly uniform films having smooth surfaces and sharp interfaces. The  $\text{Sr}_2\text{CrNbO}_6$  buffer layers on  $\text{SrTiO}_3$  (not shown) were fully strained with  $a = 3.905 \text{ \AA}$  (same as  $\text{SrTiO}_3$ ) and  $c = 3.988 \text{ \AA}$ . Consequently, the lattice constants of  $\text{Sr}_2\text{FeMoO}_6$  films grown on  $\text{Sr}_2\text{CrNbO}_6/\text{SrTiO}_3$  are almost identical to those grown directly on  $\text{SrTiO}_3$ .

Strain also plays a dominant role in determining the crystalline quality and uniformity of the  $\text{Sr}_2\text{FeMoO}_6$  films as shown by the full width at half maximum (FWHM) of the XRD rocking curves in the insets to Fig. 1 for the  $\text{Sr}_2\text{FeMoO}_6$  (004) peaks. The FWHM decreases from  $0.129^\circ$  to  $0.057^\circ$  and  $0.015^\circ$  for  $\text{Sr}_2\text{FeMoO}_6$  films on  $\text{SrTiO}_3$ ,  $\text{Sr}_2\text{GaTaO}_6$ , and  $\text{Sr}_2\text{CrNbO}_6/\text{LSAT}$  with lattice mismatch of  $-1.1\%$ ,  $0.58\%$ , and  $0.076\%$ , respectively. Clearly, the nearly perfect lattice matching between  $\text{Sr}_2\text{CrNbO}_6/\text{LSAT}$  and  $\text{Sr}_2\text{FeMoO}_6$  enables the highest crystalline quality.

Figure 2 shows the lattice constants  $a$  and  $c$  for all the  $\text{Sr}_2\text{FeMoO}_6$  films grown on the four substrates or buffer layers for  $50 \leq t \leq 200$  nm. For  $\text{Sr}_2\text{FeMoO}_6$  films on  $\text{SrTiO}_3$  and fully strained  $\text{Sr}_2\text{CrNbO}_6/\text{SrTiO}_3$ , the lattice constants show a clear strain relaxation as  $t$  increases with a quasilinear dependence, while the  $\text{Sr}_2\text{FeMoO}_6$  lattice evolves from tetragonal ( $c > a$ ) to cubic. One notes that  $a$  and  $c$  change in opposite directions during strain relaxation in order to minimize volume change of the  $\text{Sr}_2\text{FeMoO}_6$  lattice. The  $\text{Sr}_2\text{FeMoO}_6$  films at 50 nm are almost fully strained with  $a = 3.908 \text{ \AA}$  and become fully relaxed at 200 nm with  $a = 3.944 \text{ \AA}$ . For  $\text{Sr}_2\text{FeMoO}_6$

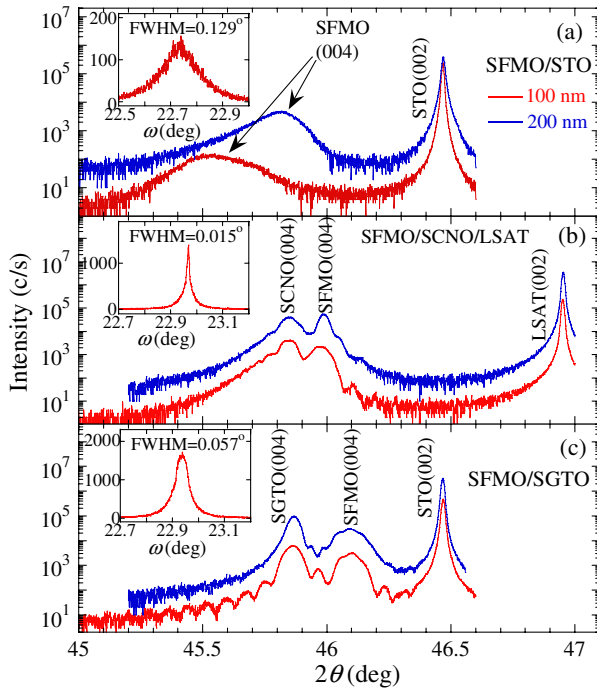


FIG. 1 (color online). Semilog  $\theta$ - $2\theta$  XRD scans of the  $\text{Sr}_2\text{FeMoO}_6$  films with thicknesses of 100 nm (red) and 200 nm (blue) grown on (a)  $\text{SrTiO}_3$ , (b)  $\text{Sr}_2\text{CrNbO}_6/\text{LSAT}$ , and (c)  $\text{Sr}_2\text{GaTaO}_6$ . The insets give the FWHM of rocking curves for the 100-nm  $\text{Sr}_2\text{FeMoO}_6$  films:  $0.129^\circ$  ( $\text{SrTiO}_3$ ),  $0.015^\circ$  ( $\text{Sr}_2\text{CrNbO}_6/\text{LSAT}$ ), and  $0.057^\circ$  ( $\text{Sr}_2\text{GaTaO}_6$ ).

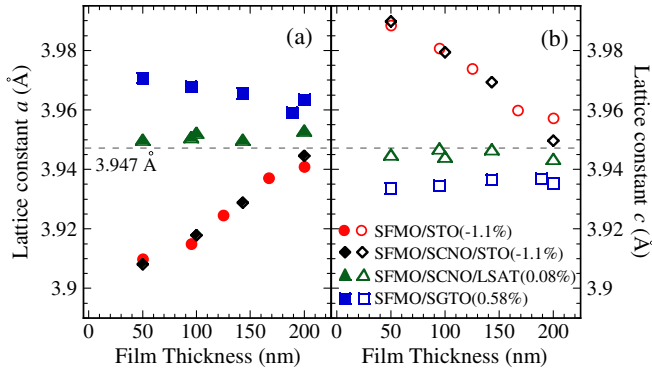


FIG. 2 (color online). Thickness dependence of (a) the in-plane lattice constant  $a$  and (b) out-of-plane lattice constant  $c$  of the  $\text{Sr}_2\text{FeMoO}_6$  films grown on  $\text{SrTiO}_3$ ,  $\text{Sr}_2\text{CrNbO}_6/\text{SrTiO}_3$ ,  $\text{Sr}_2\text{CrNbO}_6/\text{LSAT}$ , and  $\text{Sr}_2\text{GaTaO}_6$ .

films on  $\text{Sr}_2\text{CrNbO}_6/\text{LSAT}$ , because of the near perfect lattice match, the  $\text{Sr}_2\text{FeMoO}_6$  lattice is essentially cubic and strain free for all thicknesses. The  $\text{Sr}_2\text{FeMoO}_6$  films on  $\text{Sr}_2\text{GaTaO}_6/\text{SrTiO}_3$  show a slight strain relaxation with an expanded in-plane lattice constants ( $c < a$ ). At  $t = 50$  nm, the  $\text{Sr}_2\text{FeMoO}_6$  film is fully strained to  $\text{Sr}_2\text{GaTaO}_6$  with  $a = 3.970$  Å.

Ferromagnetic resonance (FMR) spectroscopy was used to measure the magnetic anisotropy of our  $\text{Sr}_2\text{FeMoO}_6$  films at 9.60 GHz with 0.2 mW input microwave power at various angles  $\theta_H$  between the dc magnetic field  $\mathbf{H}$  and the film normal [inset to Fig. 3(a)]. Fig. 3(a) shows four representative FMR spectra from a 50-nm  $\text{Sr}_2\text{FeMoO}_6$  film on  $\text{Sr}_2\text{CrNbO}_6/\text{LSAT}$  at  $\theta_H = 0^\circ, 30^\circ, 50^\circ$ , and  $90^\circ$ . The resonance field is defined as the field where the derivative of the FMR absorption crosses zero. Fig. 3(b) shows the angular dependence of the resonance field from out of plane ( $\theta_H = 0^\circ$ ) to in plane ( $\theta_H = 90^\circ$ ) for the 50-nm  $\text{Sr}_2\text{FeMoO}_6$  films on four different substrates or buffer layers, which evolves systematically as the lattice mismatch varies from  $\eta = -1.1\%$  to  $+0.58\%$ . One notes that for  $\text{Sr}_2\text{FeMoO}_6/\text{Sr}_2\text{GaTaO}_6$ , the resonant field is maximum at  $\theta_H = 90^\circ$  (in plane), indicating that the magnetic easy axis is out of plane in spite of magnetic shape anisotropy. The magnetization can be quantitatively characterized by considering the total free energy density  $F$  including Zeeman energy and anisotropy contributions. For a material with tetragonal symmetry [24,25]:

$$F = -\mathbf{H} \cdot \mathbf{M} + \frac{1}{2} M \left\{ 4\pi M_{\text{eff}} \cos^2 \theta - \frac{1}{2} H_{4\perp} \cos^4 \theta - \frac{1}{8} H_{4\parallel} (3 + \cos 4\phi) \sin^4 \theta - H_{2\parallel} \sin^2 \theta \sin^2 \left( \phi - \frac{\pi}{4} \right) \right\}, \quad (1)$$

where  $\theta$  and  $\phi$  are angles describing the orientation of the equilibrium magnetization ( $\mathbf{M}$ ) with respect to the film normal and in-plane easy axes, respectively [inset to Fig. 3(a)]. The first term in Eq. (1) is the Zeeman energy

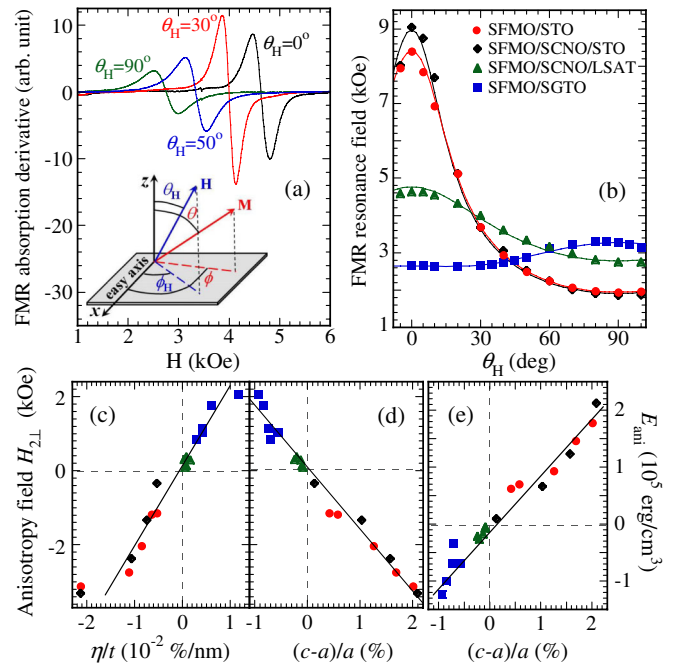


FIG. 3 (color online). (a) Room-temperature FMR derivative spectra for a 50-nm  $\text{Sr}_2\text{FeMoO}_6$  film on  $\text{Sr}_2\text{CrNbO}_6/\text{LSAT}$  at  $\theta_H = 0^\circ, 30^\circ, 50^\circ$ , and  $90^\circ$  (Inset: coordinate system used for FMR measurement and analysis) (b) Angular dependence ( $\theta_H$ ) of the resonance fields for the 50-nm  $\text{Sr}_2\text{FeMoO}_6$  films grown on  $\text{SrTiO}_3$ ,  $\text{Sr}_2\text{CrNbO}_6/\text{SrTiO}_3$ ,  $\text{Sr}_2\text{CrNbO}_6/\text{LSAT}$ , and  $\text{Sr}_2\text{GaTaO}_6$ . The fitting (solid curves) was performed using Eqs. (1) and (2) to obtain  $4\pi M_{\text{eff}}$ , from which  $H_{2\perp}$  was determined for each film. (c)  $H_{2\perp}$  of all the  $\text{Sr}_2\text{FeMoO}_6$  films as a function of  $\eta/t$  (mismatch/thickness). The solid line is the least-squares fit to all the data points excluding the two on the very left and the one on the far right ( $t = 50$  nm for all three points). (d)  $H_{2\perp}$  vs tetragonality  $(c-a)/a$  of the  $\text{Sr}_2\text{FeMoO}_6$  films. All the experimental data fall nicely onto a straight line, indicating strain-induced magnetocrystalline anisotropy. (e) Anisotropy energy  $E_{\text{ani}}$  as a function of tetragonality.

and the second term is the effective demagnetizing energy including both the shape anisotropy ( $4\pi M_s$ ) and out-of-plane uniaxial anisotropy  $H_{2\perp}$ :  $4\pi M_{\text{eff}} = 4\pi M_s - H_{2\perp}$ . Because  $M_s$  varies from sample to sample due to the effects of thickness and lattice mismatch on film quality, it was measured for each  $\text{Sr}_2\text{FeMoO}_6$  film by magnetometry. The remaining terms are out-of-plane cubic anisotropy ( $H_{4\perp}$ ), in-plane cubic anisotropy ( $H_{4\parallel}$ ), and in-plane uniaxial anisotropy ( $H_{2\parallel}$ ).

The equilibrium orientation ( $\theta, \phi$ ) can be obtained by minimizing the free energy, and the FMR resonance frequency  $\omega$  in equilibrium is given by [24–26]:

$$\left( \frac{\omega}{\gamma} \right)^2 = \frac{1}{M^2 \sin^2 \theta} \left[ \frac{\partial^2 F}{\partial \theta^2} \frac{\partial^2 F}{\partial \phi^2} - \left( \frac{\partial^2 F}{\partial \theta \partial \phi} \right)^2 \right], \quad (2)$$

where  $\gamma = g\mu_B/\hbar$  is the gyromagnetic ratio. Because  $\mathbf{M}$  is not, in general, parallel to  $\mathbf{H}$  due to shape anisotropy, we

used a numerical procedure to obtain the equilibrium angle at resonance condition [27,28]. Our experimental data for the resonance field as a function of  $\theta_H$  were fit to the expression for the free energy density at resonance to determine  $4\pi M_{\text{eff}}$ ,  $H_{4\perp}$ ,  $H_{4\parallel}$ ,  $H_{2\parallel}$ , and  $g$  factor. Figure 3(b) shows that the fitting curves agree with the experimental data very well and that  $4\pi M_{\text{eff}}$  is obviously different for  $\text{Sr}_2\text{FeMoO}_6$  films grown on the four substrates or buffer layers, while the other anisotropy terms  $H_{4\parallel}$ ,  $H_{2\parallel}$ , and  $H_{4\perp}$  are substrate-independent and comparatively small. To illustrate the effect of strain on magnetic anisotropy, Fig. 3(c) shows the linear dependence of  $H_{2\perp}$  (calculated from  $4\pi M_{\text{eff}}$  and  $M_s$ ) on lattice mismatch  $\eta$  and the inverse of film thickness  $t$ , reflecting the evolution of  $H_{2\perp}$  as strain relaxes (depending on both  $\eta$  and  $t$ ). Most of the experimental data fall on a line except for the three points for the 50-nm  $\text{Sr}_2\text{FeMoO}_6$  films on  $\text{SrTiO}_3$ ,  $\text{Sr}_2\text{CrNbO}_6/\text{SrTiO}_3$ , and  $\text{Sr}_2\text{GaTaO}_6$ , because at 50 nm, the  $\text{Sr}_2\text{FeMoO}_6$  films are below the critical thickness and fully strained as shown in Fig. 2.

This sensitivity of magnetocrystalline anisotropy to lattice symmetry highlights a key result of our study: the striking proportionality of  $H_{2\perp}$  to the tetragonality of the  $\text{Sr}_2\text{FeMoO}_6$  lattice over a broad range ( $-0.93\% < (c - a)/a < +2.0\%$ ),

$$H_{2\perp} = (32 \pm 60) - (162.7 \pm 5.9) \times 10^3 \times [(c - a)/a] (\text{Oe})$$

as shown in Fig. 3(d), demonstrating a fundamental relationship between magnetocrystalline anisotropy and lattice symmetry.

The strain-induced anisotropy arises from the magnetoelastic effect [29,30] in which a change in interatomic distances alters the magnetic properties through spin-orbit coupling. The magnetoelastic energy density is given by  $F = -\sigma b \cos^2 \alpha$ , where  $b$  is the magnetoelastic constant,  $\sigma$  the tetragonality  $(c - a)/a$ , and  $\alpha$  the angle between  $\mathbf{M}$  and strain direction. When  $\mathbf{M}$  is along the [001] direction,  $F = -\sigma b$ . Figure 3(e) shows the linear dependence of anisotropy energy,

$$E_{\text{ani}} = -\frac{1}{2} M H_{2\perp}, \quad (3)$$

on tetragonality for all  $\text{Sr}_2\text{FeMoO}_6$  films, from which a least-squares fit gives,

$$E_{\text{ani}} = (-5.0 \pm 4.6) \times 10^3 + (92.9 \pm 4.5) \times 10^5 \\ \times [(c - a)/a] (\text{erg/cm}^3).$$

The slope of the line in Fig. 3(e) gives  $-b = (92.9 \pm 4.5) \times 10^5 \text{ erg/cm}^3$ . The negative value of  $b$  implies that the magnetic easy axis is parallel to

the short axis of the tetragonal lattice. The ability to tune the magnetization using both thickness and substrates brings in precise control in fabricating a spintronic device.

The variation of  $H_{2\perp}$  with tetragonal distortion of  $\text{Sr}_2\text{FeMoO}_6$  results in evolution of the total magnetic anisotropy and, most interestingly, perpendicular anisotropy in  $\text{Sr}_2\text{FeMoO}_6$  films on  $\text{Sr}_2\text{GaTaO}_6/\text{SrTiO}_3$  by overcoming the demagnetizing field (see the magnetic hysteresis loops in Fig. S1, Supplemental Material [31]). The saturation field ( $H_s$ ) of the out-of-plane hysteresis loops depends on  $4\pi M_{\text{eff}} = 4\pi M_s - H_{2\perp}$ . For a 100-nm  $\text{Sr}_2\text{FeMoO}_6$  film on  $\text{SrTiO}_3$  [Fig. S1(a)],  $4\pi M_s = 1343 \text{ Oe}$  and  $H_{2\perp} = -2737 \text{ Oe}$ , resulting in a  $4\pi M_{\text{eff}} = 4080 \text{ Oe}$ , which matches well with the  $H_s$  of the out-of-plane hysteresis loop. For  $\text{Sr}_2\text{FeMoO}_6/\text{Sr}_2\text{CrNbO}_6/\text{LSAT}$  [Fig. S1(b)],  $H_{2\perp}$  is almost zero and  $4\pi M_{\text{eff}} \approx 4\pi M_s = 1525 \text{ Oe}$ , which agrees with the observed  $H_s$ . For  $\text{Sr}_2\text{FeMoO}_6/\text{Sr}_2\text{GaTaO}_6$  [Fig. S1(c)],  $H_{2\perp} = +1753 \text{ Oe}$ , which is large enough to compensate the demagnetizing field  $4\pi M_s = 1430 \text{ Oe}$ , resulting in a negative  $4\pi M_{\text{eff}} = -323 \text{ Oe}$  and, consequently, an out-of-plane easy axis. Thus we have demonstrated the ability to shift the magnetic easy axis from in plane to out of plane via epitaxial strain in  $\text{Sr}_2\text{FeMoO}_6$ .

The strong magnetocrystalline anisotropy and high  $T_C$  in  $\text{Sr}_2\text{FeMoO}_6$  and other compounds (e.g., containing  $5d$  transition metals) with strong spin-orbit coupling provide unique opportunities for studying strain-induced magnetoelastic coupling and point toward potentially important spintronic applications that build on the ability to control magnetism through modification of lattice parameters. FMR measurements reveal a surprisingly straightforward linear dependence of magnetocrystalline anisotropy on the tetragonality of  $\text{Sr}_2\text{FeMoO}_6$ , implying the opportunity to gain detailed understanding of the magnetoelastic interaction that will enhance the value of this material for spintronics research and technology. Our results demonstrate that the magnetocrystalline anisotropy can be tuned through strain engineering over a broad range of values sufficient to switch from in-plane to out-of-plane magnetization states even in zero applied fields. This implies that  $\text{Sr}_2\text{FeMoO}_6$  films grown on piezoelectric substrates or underlayers could be electrically switched for novel room-temperature spintronic applications.

This work is supported by the Center for Emergent Materials at the Ohio State University, a NSF Materials Research Science and Engineering Center (DMR-0820414) (H.L.W., A.J.H., and F.Y.Y.) and by the Department of Energy through Grant No. DE-FG02-03ER46054 (R.A. and P.C.H.). Partial support is provided by Lake Shore Cryogenics Inc. (C.H.D.) and the NanoSystems Laboratory at the Ohio State University.

\*fyyang@physics.osu.edu

†hammel@physics.osu.edu

- [1] S. A. Wolf, D. D. Awschalom, R. A. Buhrman, J. M. Daughton, S. von Molnár, M. L. Roukes, A. Y. Chtchelkanova, and D. M. Treger, *Science* **294**, 1488 (2001).
- [2] K. L. Kobayashi, T. Kimura, H. Sawada, K. Terakura, and Y. Tokura, *Nature (London)* **395**, 357 (1998).
- [3] D. Serrate, J. M. De Teresa, and M. R. Ibarra, *J. Phys. Condens. Matter* **19**, 023201 (2007).
- [4] A. W. Sleight and J. F. Weiher, *J. Phys. Chem. Solids* **33**, 679 (1972).
- [5] O. Erten, O. Nganba Meetei, A. Mukherjee, M. Randeria, N. Trivedi, and P. Woodward, *Phys. Rev. Lett.* **107**, 257201 (2011).
- [6] T. Manako, M. Izumi, Y. Konishi, K.-I. Kobayashi, M. Kawasaki, and Y. Tokura, *Appl. Phys. Lett.* **74**, 2215 (1999).
- [7] S. Q. Wang, H. Y. Pan, X. P. Zhang, G. J. Lian, and G. C. Xiong, *Appl. Phys. Lett.* **88**, 121912 (2006).
- [8] D. Sanchez, M. Garcia-Hernandez, N. Auth, and G. Jakob, *J. Appl. Phys.* **96**, 2736 (2004).
- [9] M. Osugi, H. Asano, D. Hidashida, and M. Matsui, *J. Magn. Soc. Jpn.* **25**, 887 (2001).
- [10] A. J. Hauser, R. E. A. Williams, R. A. Ricciardo, A. a Genc, M. Dixit, J. M. Lucy, P. M. Woodward, H. L. Fraser, and F. Yang, *Phys. Rev. B* **83**, 014407 (2011).
- [11] T. Nosach, G. Mullady, N. Leifer, V. Adyam, Q. Li, S. Greenbaum, and Y. Ren, *J. Appl. Phys.* **103**, 07E311 (2008).
- [12] M. Bibes and A. Barthélémy, *Appl. Phys. Lett.* **83**, 2629 (2003).
- [13] H. Asano, N. Koduka, K. Imaeda, M. Sugiyama, and M. Matsui, *IEEE Trans. Magn.* **41**, 2811 (2005).
- [14] D. C. Ralph and M. D. Stiles, *J. Magn. Magn. Mater.* **320**, 1190 (2008).
- [15] A. D. Kent, B. Özyilmaz, and E. del Barco, *Appl. Phys. Lett.* **84**, 3897 (2004).
- [16] D. Houssameddine *et al.*, *Nat. Mater.* **6**, 447 (2007).
- [17] B. Heinrich, K. Urquhart, A. Arrott, J. Cochran, K. Myrtle, and S. Purcell, *Phys. Rev. Lett.* **59**, 1756 (1987).
- [18] M. Kowalewski, C. M. Schneider, and B. Heinrich, *Phys. Rev. B* **47**, 8748 (1993).
- [19] S. Kim, H. Lee, T. Yoo, S. Lee, S. Lee, X. Liu, and J. K. Furdyna, *J. Appl. Phys.* **107**, 103911 (2010).
- [20] M. Cubukcu, H. J. von Bardeleben, Kh. Khazen, J. L. Cantin, O. Manguin, L. Largeau, and A. Lemaître, *Phys. Rev. B* **81**, 041202(R) (2010).
- [21] C. Kwon, S. E. Lofland, S. M. Bhagat, M. Rajeswari, T. Venkatesan, R. Ramesh, A. R. Kratz, and R. D. Gomez, *IEEE Trans. Magn.* **33**, 3964 (1997).
- [22] A. J. Hauser *et al.*, *Phys. Rev. B* **85**, 161201(R) (2012).
- [23] A. J. Hauser, J. M. Lucy, H. L. Wang, J. R. Soliz, A. Holcomb, P. Morris, P. M. Woodward, and F. Y. Yang, *Appl. Phys. Lett.* **102**, 032403 (2013).
- [24] X. Liu, W. L. Lim, L. V. Titova, M. Dobrowolska, J. K. Furdyna, M. Kutrowski, and T. Wojtowicz, *J. Appl. Phys.* **98**, 063904 (2005).
- [25] M. Farley, *Rep. Prog. Phys.* **61**, 755 (1998).
- [26] H. Suhl, *Phys. Rev.* **97**, 555 (1955).
- [27] Y. Q. He and P. E. Wigen, *J. Magn. Magn. Mater.* **53**, 115 (1985).
- [28] X. Liu, Y. Sasaki, and J. K. Furdyna, *Phys. Rev. B* **67**, 205204 (2003).
- [29] C. Chappert and P. Bruno, *J. Appl. Phys.* **64**, 5736 (1988).
- [30] R. Zuberek, K. Fronc, A. Szewczyk, and H. Szymczak, *J. Magn. Magn. Mater.* **260**, 386 (2003).
- [31] See Supplemental Material at <http://link.aps.org/supplemental/10.1103/PhysRevLett.110.147204> for the in-plane and out-of-plane magnetic hysteresis loops of the Sr<sub>2</sub>FeMoO<sub>6</sub> films on three different substrates or buffer layers.